Solar Energy Materials & Solar Cells 209 (2020) 110470

Contents lists available at ScienceDirect

Solar Energy Materials and Solar Cells

journal homepage: http://www.elsevier.com/locate/solmat

Eliminating light- and elevated temperature-induced degradation in *P*-type PERC solar cells by a two-step thermal process

Chandany Sen *, Catherine Chan, Phillip Hamer, Matthew Wright, CheeMun Chong, Brett Hallam, Malcolm Abbott

School of Photovoltaic and Renewable Energy Engineering, University of New South Wales, Sydney, NSW, 2052, Australia

ARTICLE INFO

Keywords:
Two-step thermal process
Multi-crystalline silicon (mc-Si)
Light- and elevated temperature-induced degradation (LeTID)
Contact resistance
Eliminating

ABSTRACT

Light- and elevated temperature-induced degradation (LeTID) can have a severe impact on the carrier lifetime of silicon substrates used in solar cell production and thus remains a crucial challenge for manufacturers. In this work, we introduce a two-step annealing process to mitigate LeTID in multi-crystalline silicon (mc-Si) passivated emitter and rear cell (PERC) solar cells. We demonstrate that the first annealing step (450 °C) with a slow belt speed (0.5 m/min) plays a primary role in mitigating LeTID in the cells, but also results in an increase in contact resistance. The application of a second annealing step at a similar temperature (400–500 °C) with a faster belt speed (1.4 m/min) recovers the contact resistance whilst maintaining the stability of the cell. Applying this approach to the *p*-type mc-Si PERC solar cells resulted in a reduction of efficiency loss during light soaking from ~6%$_{rel}$ (control) to ~1%$_{rel}$ (treated sample). This finding is significant for *p*-type mc-Si solar cell manufacturers, as the process can be applied to finished cells using a standard belt firing furnace to stabilise cell efficiency for long term operation in the field.

1. Introduction

Silicon solar cells suffer from light- and elevated temperature-induced degradation (LeTID), which cannot be attributed to boron-oxygen (B–O) or iron-boron (Fe–B) complexes [1]. This degradation was first reported by Ramspeck et al. in 2012 [1], and the term LeTID was introduced by Kersten et al. in 2015 [2]. LeTID has been observed to affect all types of silicon materials including *p*-type (B-doped and Ga-doped) and *n*-type silicon, fabricated using a variety of methods including float zone (FZ), Czochralski (Cz), cast-mono, and multi-crystalline silicon (mc-Si) [1,3–6]. The extent of LeTID in *p*-type cast-mono and mc-Si is, however, reported to be much more significant than that of other materials, especially in passivated emitter and rear cell (PERC) solar cells [1,5]. In the past, it was reported that LeTID caused performance losses of ~10–12%$_{rel}$, depending on the bulk material, position in the ingot and the solar cell processing [7]. Recently, it has been reported that the extent of LeTID has been suppressed to between 1-2%$_{rel}$ [8–10,61]; however, the ultimate goal is to completely remove performance losses associated with LeTID.

Many research groups have investigated this phenomenon; however, the exact root cause of the degradation still remains unclear [3,5, 11–16]. Several research institutions (including our own) have shown evidence that LeTID is caused by a bulk defect, possibly related to excessive hydrogen in the bulk [17–24]. To suppress this degradation, several approaches have been introduced, including using high-intensity laser illumination [25,26], reducing the peak metallisation firing temperature [27–29], reducing the cooling rate of the metallisation firing process [21,30,31], tuning of the SiN_x:H layer thickness [14,24] and composition [14,32], reducing the wafer thickness [33], and applying pre- and post-fire annealing processes [9,31,34–36]. These processes are thought to limit the amount of hydrogen in the bulk and/or to convert hydrogen in the bulk into more stable forms that are no longer able to cause LeTID. However, many of these processes either do not fully mitigate LeTID, require compromises in cell design or are otherwise incompatible with commercial production processing.

Post-fire thermal processing has previously been used to suppress LeTID in *p*-type mc-Si [27,35–37]. Sharma et al. demonstrated that by applying dark annealing after fast-firing at 550 °C for 20 min, the extent of lifetime degradation could be reduced by 20% [37]. Similarly, Yli-Koski et al. reported that post-fire dark annealing at 300 °C for 40 h could almost fully suppress the degradation of V_{OC} in PERC cell [36]. However, both of these processes are too long to incorporate into the

* Corresponding author.
E-mail address: chandany.sen@unsw.edu.au (C. Sen).

https://doi.org/10.1016/j.solmat.2020.110470
Received 25 December 2019; Received in revised form 12 February 2020; Accepted 12 February 2020
Available online 19 February 2020

solar cell production line. In 2018, our group showed that LeTID measured on a lifetime test structure could be completely mitigated after applying post-fire annealing at 450 °C for ~1 min with a prolonged cooling rate of ~2 °C/s using rapid thermal processing (RTP) [35]. Although post-fire annealing has been shown to effectively eliminate LeTID in lifetime test structures, such processes were found to have a detrimental impact on the fill factor (FF) and efficiency (η) of completed solar cells. In particular, the processes caused the front silver contact resistance to increase severely [38,39]. A similar increase of contact resistance was seen in other work where it was attributed to a thickening of the interfacial glass layer, which forms part of the screen print contact [40]. However, we have also observed that the application of reverse bias to the cell causes a permanent recovery of the contact, which is difficult to explain via a thickening of the glass [39,41]. Currently, the problem of increased contact resistance has prevented the use of a rapid post-firing anneal to mitigate LeTID in industrial PERC solar cells.

This paper shows that this increase in contact resistance is also reversible by applying a second rapid thermal process. Thus, an approach to eliminate LeTID in *p*-type mc-Si PERC cells is proposed, which combines two post-fire annealing steps. Firstly, annealing with a slower belt speed (longer duration) to completely mitigate the LeTID, then, reannealing with a faster belt speed (shorter duration) to eliminate the increased R_s induced by the LeTID treatment process. The impact of these processes on cell performance, lifetime and LeTID are explored. This approach requires a short process time (~3 min) and thus may be potentially able to apply in the solar cell production line to eliminate LeTID.

2. Methodology

High performance (HP) *p*-type mc-Si PERC cells were sourced from industrial production lines at two different companies (referred to herein as Manufacturer A and Manufacturer B). Cells from Manufacturer A had not received any post-production processes to mitigate LeTID. The cells from Manufacturer B included two groups, the first group had received post-production LeTID treatment (via current injection at elevated temperature), and the second group had not. Manufacturer B also supplied PERC precursors (i.e. samples prepared without metallisation or rear-side laser ablation and did not received any firing process).

The cells from Manufacturer A were cleaved with a laser into 32 mm × 32 mm tokens for some of the experimental work in this manuscript. The first annealing step was performed in a commercial inline firing furnace (SierraTherm) at a set temperature of 450 °C with a belt speed of 0.5 m/min. The second annealing step was performed in the same furnace, with the set temperatures ranging from 400 °C to 700 °C with a constant belt speed of 1.4 m/min. The actual cell temperature profiles were measured on identical dummy samples using a Q18 Datapaq thermal profiler that was averaged using three K-type thermocouples (Omega SCAXL-IM050G-150). The long duration required for stability testing (>1000 h) limited the number of samples at each condition to two or three tokens per condition. All samples were then subjected to a stability test at a sample temperature of 75 °C, with a broadband halogen source emitting an irradiance of 1000 ± 15 W/m^2 at the sample level. Fig. 1a shows a flow diagram of the experiment process sequence and (b) illustrates the time and sample temperature profiles of the first and second annealing processes.

The PERC precursors (sourced from Manufacturer B) were used to determine if the change in V_{OC} after each processing step was related to changes in the bulk and/or surface. For this group, after depositing the AlO_x:H and SiN_x:H layers, the samples were laser cleaved into 52 mm × 52 mm tokens. The samples underwent a fast-firing at an actual wafer temperature of ~750 °C with a belt speed of 4.5 m/min using the same infrared firing furnace described above, to provide a similar thermal history to the cells (i.e. to replicate the impact of contact firing). Note that the firing profile for this group of samples may not be identical to that used for the cells. This was followed by the first and second annealing treatment, as described in Fig. 1a. All samples were then light-soaked at 130 °C with a broadband halogen source emitting an irradiance of 1000 ± 15 W/m^2 at the sample level. This stability testing condition was chosen as it has been shown that if light-soaked was carried at the temperature ≤150 °C, it induced similar LeTID extent to the conventional light soaking condition (75 °C, 1000 W/m^2); however, the degradation and regeneration kinetics are accelerated [4].

All solar cell tokens were periodically characterised using current-voltage (I–V) testing under STC (1 sun and 25 °C) conditions using a custom-built I–V tester, with a halogen light source. I–V measurements were performed after firing (initial), each post-fire annealing step, and at incremental steps during the stability test. The open-circuit voltage (V_{OC}) and pseudo-FF (pFF) were measured using a Suns-V_{OC} tool from Sinton Instruments [42]. The series resistance (R_s) was calculated by comparing the Suns-V_{OC} curve with the one-sun I–V curve [43]. The front contact resistivity was measured on selected samples by the transfer length method (TLM) [44]. In this case, the sample was laser cleaved from the rear side into 5 mm wide strips.

For all PERC precursors, the lifetime measurements were carried out using a quasi-steady-state photoconductance lifetime tester (Sinton Instruments WCT-120) at 30 °C on samples after firing, first annealing, second annealing and after incremental steps during stability testing [45]. The generalized technique was used to analyse the data [46]. The intrinsic recombination was corrected for Auger recombination using the Richter model [47]. Injection level-dependent lifetime spectroscopy (IDLS) analysis was performed to extract injection-dependent Shockley-Read-Hall (SRH) bulk recombination related lifetime (τ_{SRH}), emitter saturation current density (J_{0e}) and electron-hole capture cross-section ratio (k-value) using the same fitting method and assumptions

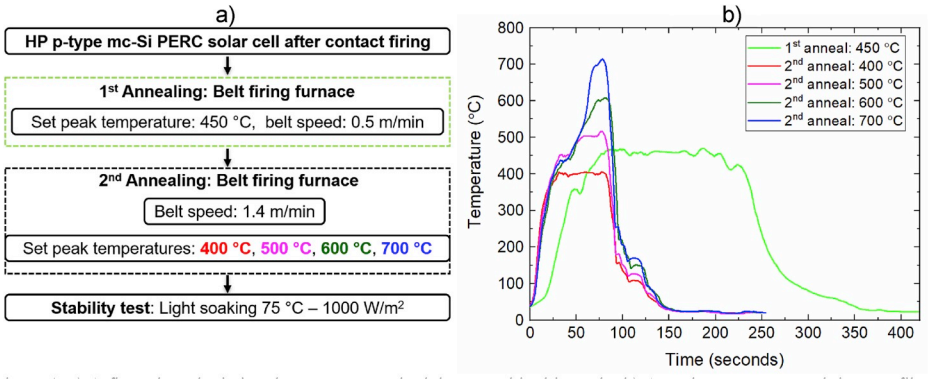

Fig. 1. a) A flow chart depicting the two-step methodology used in this study. b) Actual temperature and time profiles used in this study for the first annealing at 450 °C with belt speed 0.5 m/min and second annealing at the set temperatures of 400 °C–700 °C with a belt speed of 1.4 m/min.

described in Ref. [35]. We note that as described in Ref. [35], to achieve the goodness-of-fit metric for the entire injection ranges, a constant value of bulk lifetime at all injection levels ($\tau_{bulk,const}$), which represents all of the other bulk recombination related lifetime sources within the material was included in the fitting.

Photoluminescence (PL) images of the selected samples (control sample, and samples that underwent the first and second annealing steps at 400 °C and 700 °C) were taken using BTi (LIS-R3) luminescence imaging system. The PL images were captured on the tokens after firing, after the first and second treatment, and at the most degraded point, which occurred at ~19 h of light soaking at 130 °C with 1000 W/m^2 illumination intensity. PL ratio images at each processing step were created by comparing the image before treatment (firing) and after each annealing step, and after the point of maximum degradation using image comparison and registration user software (ICARUS) [48].

An optimised process (first annealing at 450 °C and second annealing at 400 °C) identified in the early experiments on tokens was applied to the non-treated LeTID full-area PERC cells sourced from Manufacturer B. The same stability testing as described above was applied to these treated samples. Also included were two cells that did not receive any treatment and two LeTID treated cells (i.e. cells which were treated by Manufacturer B). For the full area cells, the IV measurements after incremental steps during the stability test were performed using the LOANA solar cell characterization tool (pv-tools, Germany).

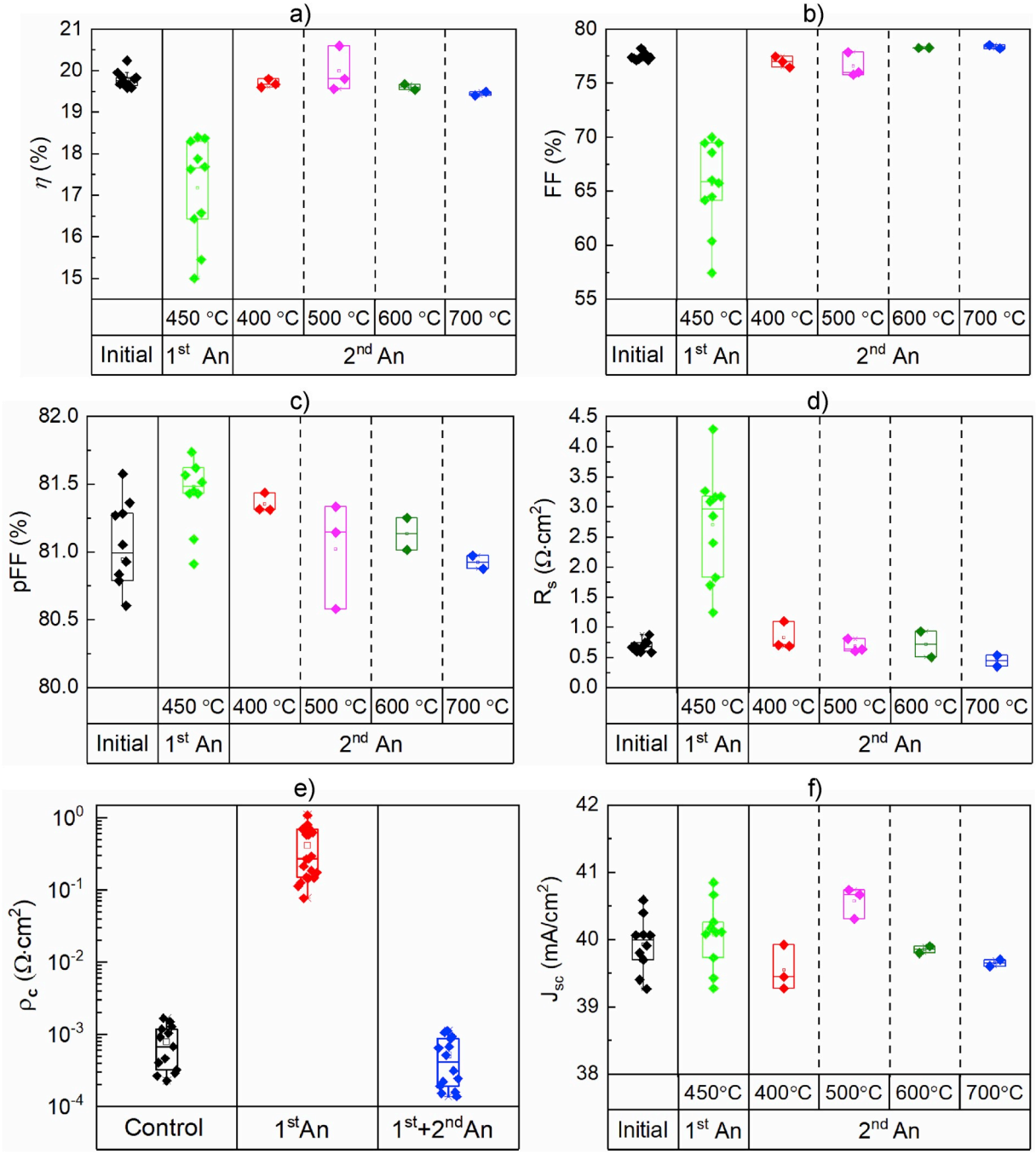

Fig. 2. Changes in a) η, b) FF, c) pFF, and d) R_s after the first and second annealing process, e) Contact resistivity of the control sample, the sample that underwent first annealing (450 °C) only, and the sample that underwent first (450 °C) and second annealing at 700 °C and f) J_{sc}. The first and second annealing steps were performed with a belt speed of 0.5 m/min and 1.4 m/min, respectively. "An" means annealing. These samples were sourced from Manufacturer A.

3. Results

3.1. Immediate impact of annealing steps on cell performance

Directly after processing (i.e. prior to light soaking), the annealing steps were found to have a significant impact on cell efficiency. Fig. 2a presents the changes in η after the first and second annealing treatments. The first annealing process caused a severe drop in cell efficiency, ranging between ~1%$_{abs}$ to ~5%$_{abs}$, which is equivalent to ~5%$_{rel}$, and ~25%$_{rel}$, respectively, despite all samples being treated with the same conditions. The significant loss of η after the first annealing step was clearly due to an increased series resistance in the cells (see Fig. 2d). No significant decrease in pFF was observed (Fig. 2c), indicating no additional recombination or shunting impacted the FF. Measurement of the contact resistance confirmed this increase to be due to severely increased contact resistance, similar to the previously observed results [38–41,49]. Note that the tokens had different starting cell efficiency values, ranging from ~19.5% to ~20.2%, likely due to the different bulk defect density in the mc-Si wafers, uniformity of cell processing and/or the amount of damage induced by the laser cleaving process.

The amount of recovery of the efficiency following the second rapid treatment was dependent on the temperature. For temperatures ≤500 °C, the η recovered to the initial values and/or slightly higher (~1.8%$_{rel}$). Increasing the temperature during the second annealing step to >500 °C reduced the amount of recovery observed with the second process. The relative loss was ~2.5%$_{rel}$ after a second treatment at 700 °C. In all cases, this recovery was driven by a reduction in contact resistance, reduction in series resistance and thus recovery of the FF. There was no significant change in short circuit current density (J_{sc}) after the first and second annealing, the change was within ~ ± 0.3 mA/cm^2 (~±1%$_{rel}$), which is within the error of the custom-built I–V tester (see Fig. 2f).

The dependence of the final cell efficiency on the second annealing temperature was due to variations in V_{OC} of the cells after processing (see Fig. 3a). The cell V_{OC} showed significant scatter (from 635 mV to 652 mV) likely due to non-uniformity of bulk defect density in the mc-Si wafers. To enable better comparison the relative values (calculated as a change in V_{OC} divided by initial V_{OC} for each cell) are plotted in Fig. 3b. After the first annealing step (450 °C for all samples) the V_{OC} increased by ~0.5%$_{rel}$ (~3–4 mV). After the second treatment at lower temperatures ≤500 °C, the V_{OC} remained almost constant, while there was a decrease in V_{OC} up to ~1.5%$_{rel}$ after the second annealing step at higher temperatures >500 °C. The changes in V_{OC} after both treatments were observed to correlate with the evolution of bulk lifetime, which will be discussed in more detail in section 3c. In addition, the drop of the V_{OC} after second annealing at high temperatures ≥600 °C was also likely due to re-melting, and re-crystallising of the p^+ BSF as this temperature is higher than Aluminium and Si eutectic temperature [50].

3.2. Impact of annealing steps on cell stability

The stability of the cells was substantially impacted by the peak temperature of the second annealing step. Fig. 4a and b shows the evolution of V_{OC} and η after the first and second annealing steps and after incremental steps of light soaking. After the light soaking, the control sample suffered a severe degradation compared to that of the treated samples. The V_{OC} degraded by ~27 mV (~4.5%$_{rel}$) and the η dropped by 2%$_{abs}$ (~10%$_{rel}$) after ~200 h (maximum degradation point) of light soaking. After this point, a slow recovery was observed. However, the efficiency did not fully recover to its original value, even after more than ~1700 h of light soaking. On the other hand, there was no degradation in V_{OC} of the token that underwent the first annealing only; however, this process caused a significant loss in η of ~6%$_{abs}$ (18%$_{rel}$) due to the increase in front contact resistivity after the first annealing process. For samples with two annealing processes, after light soaking, there was a significant drop in V_{OC} and η as the temperature of the second annealing process was increased. The sample that underwent second annealing at 400 °C showed recovery in efficiency after the second treatment step, and interestingly, there was no significant degradation for both V_{OC} and η observed after more than 1700 h of light soaking. The V_{OC} and η of the token that underwent the second annealing step at 500 °C increased after the treatment. Although it slightly degraded after light soaking, the V_{OC} and η remained closed to its original values. Increasing the second annealing temperatures to ≥600 °C resulted in some recovery of the efficiency; however, there was a ~19 mV (~3%$_{rel}$) loss in V_{OC}. No significant recovery was observed for all tokens that underwent second treatment at higher temperatures (≥600 °C).

3.3. Impact of annealing steps on PERC precursors

3.3.1. Changes in bulk lifetime and emitter saturation current density

The results from the lifetime test structures indicated that changes in cell V_{OC} were caused by changes in the bulk lifetime rather than surface lifetime. Fig. 5 shows the changes in τ_{SRH} and J_{0e} after the first annealing, the second annealing and after incremental steps of light soaking. After the first treatment, there was a significant increase in τ_{SRH}, whilst the total J_{0e} was only slightly affected; the change was within ~5–10% of the initial value. The improvement of the τ_{SRH} was consistent with the observed increase in V_{OC} on the small cells (see Figs. 3 and 4a), implying that the increase of V_{OC} after first annealing was primarily because of the bulk improvement. This result was as expected and aligns closely with our previous work demonstrating that post-fire thermal processes improved bulk lifetime significantly [35]. The improvement in lifetime after the post-fire thermal process has also been observed by other researchers [51–53]. After the second treatment at lower temperatures of ≤500 °C, τ_{SRH} and J_{0e} did not change significantly. Increasing the second annealing temperature to >500 °C, caused

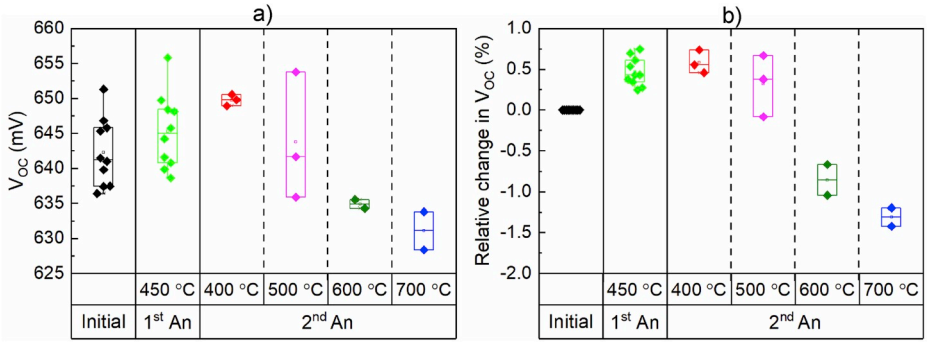

Fig. 3. Changes in a) absolute V_{OC} after the first annealing and the second annealing steps. b) Relative change in V_{OC} compared to the initial values. "An" means annealing. These samples were sourced from Manufacturer A.

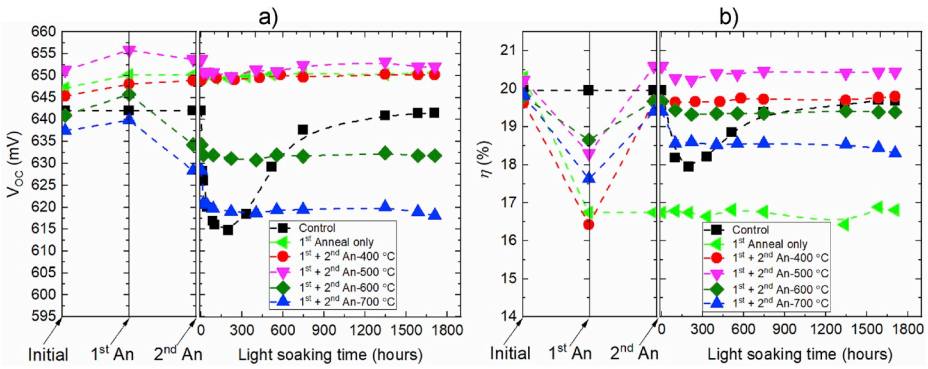

Fig. 4. Evolution of a) V_{OC} and b) η after the first annealing, second annealing, and light soaking. The stability testing condition was 75 °C with an illumination intensity of 1000 W/m^2 "An" means annealing. All samples were sourced from Manufacturer A.

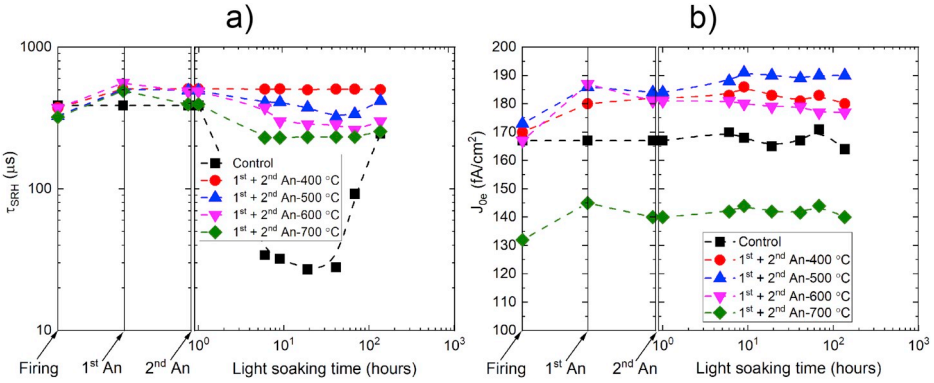

Fig. 5. Change in a) bulk lifetime (τ_{SRH}) and b) emitter saturation current (J_{0e}) annealing and light soaking. The stability testing condition was 130 °C with an illumination intensity of 1000 W/m^2 "An" means annealing. All samples were sourced from Manufacturer B.

a reduction in τ_{SRH}, leading to an observed decrease in V_{OC} in the tokens (small cells) see Figs. 3 and 4a. On the other hand, the J_{0e} was slightly improved after the second treatment at high temperatures.

Light soaking resulted in a degradation of the bulk lifetime but did not cause a substantial change in J_{0e} of the control or the treated samples. The τ_{SRH} of the control sample degraded from ~400 µs to ~30 µs, whilst for the sample that underwent second annealing at 700 °C, the τ_{SRH} dropped from ~400 µs to ~250 µs after 19 h of light soaking, the maximum degradation point of light soaking at 130 °C with 1000 W/m^2 illumination intensity. The τ_{SRH} of the samples that underwent annealing at lower temperatures (400 °C) remained stable. These results indicate that the drop of the VOC and η of the control and the samples that underwent second annealing at higher temperature is caused by a bulk defect.

3.3.2. Changes in PL images and SRH properties. Changes in PL images provide additional information on the localised evolution of lifetime after each processing and degradation step. Fig. 6 shows the open-circuit PL images, and PL ratio mapping of the control sample and the samples that underwent the first annealing at 450 °C followed by the second annealing at 400 °C and 700 °C. We note that different PL ratio scales were used to better visualise the localised impact of the samples. After the first annealing, PL counts improved significantly, primarily at the grain boundaries, and dislocations. This result is consistent with the observed increase in τ_{SRH} and V_{OC} and suggests that the first annealing process may have enhanced bulk hydrogenation mainly at the high recombination areas. However, there was no substantial change in PL counts after the second annealing at 400 °C, while for the sample that underwent second annealing at 700 °C, PL counts dropped significantly.

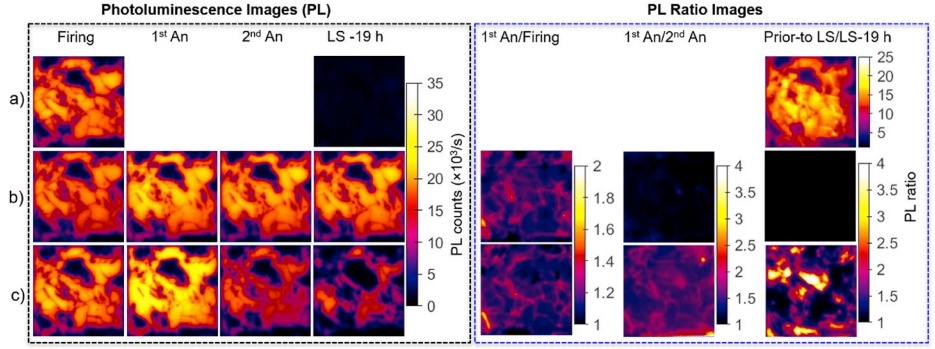

Fig. 6. PL and PL ratio images of the a) control sample and sample that underwent the first annealing at 450 °C followed by second annealing at b) 400 °C and c) 700 °C. "An" means annealing. These samples were sourced from Manufacturer B.

The reduction in PL counts occurred relatively uniformly throughout the samples.

The control sample (Fig. 6a) exhibited a substantial drop in the PL counts after 19 h of light soaking. The reduction was more pronounced in the higher lifetime areas, and the maximum reduction was up to a factor of ~20, which was much more severe than the treated samples. PL counts of the sample that underwent the second treatment at 400 °C (Fig. 6b) did not change after illumination, while there was a slight drop in PL counts observed in the sample that underwent second annealing at 700 °C (Fig. 6c). Unlike the control sample, this degradation of the sample that underwent second annealing at 700 °C was localized in heavily dislocated areas, and the relative loss of PL counts was within a factor of ~3–4. This observation of LeTID localised within the dislocated regions of a sample has been observed previously for samples with lower hydrogen content dielectrics [34].

Detailed curve fitting of the injection-dependent lifetime data supported the stability of the surface and degradation of the bulk due to LeTID. Detailed curve fitting analysis for a control lifetime structure and a sample that underwent a second annealing step at 700 °C are shown in Fig. 7. After light soaking, there were no significant changes in J_{0e} and $\tau_{bulk,cont}$ of both the control and treated samples. However, light soaking caused τ_{SRH} of the control and treated samples to degrade, although the degradation extent of the control sample was significantly higher. As shown in the inset of Fig. 7a and b, the k-value of the control sample before and after degradation was approximately the same (firing ~31 ± 8 and light soaking ~38 ± 2) and was the same as those of the treated sample (second annealing ~30 ± 3 and light soaking ~37 ± 6), indicating that the defect was already pre-formed during firing and second annealing at high temperature. These k-values are in the range of previously reported k-values for the LeTID defect [3,16,28,54,55], suggesting that the degradation of control and treated samples was caused by the LeTID defect. This result indicates that the degradation within the samples fired at the higher temperatures is likely due to a re-introduction of LeTID in the bulk of the material (note that in the second case it is occurring in localised regions as per the PL images) (see Fig. 6c).

3.4. Application to large area PERC solar cells

Application of the optimised annealing recipe to full area PERC solar cells resulted in improved stability. Fig. 8 presents the changes in the V_{OC} and η relative to the initial values. The control samples, which did not receive any treatment, experienced a significant reduction in both V_{OC} and η. The losses were scattered between ~1.5%$_{rel}$ to ~2%$_{rel}$ for V_{OC} and between ~4%$_{rel}$ to ~6%$_{rel}$ for η. The scatter in degradation extent was likely due to the different defect density of the bulk material and non-uniformity of the cell processing from the production line. However, for cells treated using the method proposed in this work, degradation in V_{OC} and η were limited to ≤0.5%$_{rel}$ and ≤1%$_{rel}$, respectively. These extents of degradation remained relatively lower than that of the degradation observed in the samples that were treated by Manufacturer B (V_{OC} loss was ~1%$_{rel}$, and η loss was ~2.5%$_{rel}$). This result indicates that this treatment has effectively suppressed the degradation in the full-size industrial cells by up to ~70% (for V_{OC}) and ~80% (for η). To improve the effectiveness of this treatment on full-large area cells, further optimization may be required. A study involving a larger set of samples that covers a greater range of mc-Si material inhomogeneities is also required to assess its impact throughout a typical silicon brick.

4. Discussion

4.1. Recovery of contact resistance

This work showed that the second annealing process recovered the increase in contact resistance caused by the first annealing step. This recovery occurred even when the same peak temperature range (400–500 °C) was applied. This result is very surprising in the context of our earlier work, which found that the degradation of contact resistance occurred at these annealing temperatures [38,41] and that previous applications of rapid cooling (annealing with a hotplate) did not fix the contact issue [39,41]. This implies that something more complex than simply the peak temperature or cooling rate alone is involved in the degradation and recovery of contact resistance. It may rather be related to the total thermal budget, i.e. a combination of peak temperature, heating/cooling profile and annealing duration applied. Without further studies, it is not possible to draw any definite conclusions about what the underlying process difference was that ultimately resulted in the recovery. We do, however, make note of two significant differences in this work compared to earlier studies. Firstly is the use of a double process, resulting in cooling the sample before reheating. Secondly is differences in the heating and cooling rates that were not constant with time. The second point occurs due to the use of a belt furnace with a fixed speed that moves the wafer through the thermal zones and ultimately into the cooling zone. Future work should involve detailed studies to distinguish the role of peak temperature, heating/cooling profile and annealing duration on the deterioration and recovery of the contact resistance.

The results of this work provide some further insight into the hypothesis proposed in previous studies of the increased contact resistance problem. Firstly, the results here do not appear to support a thickening of the interfacial glass layer. It is hard to explain how further thermal processing (which would only serve to increase that thickness) would then result in a recovery. The implications for the role of hydrogen in the increase of contact resistance are less clear. Future work using modelling of hydrogen in silicon should attempt to account for this observed result.

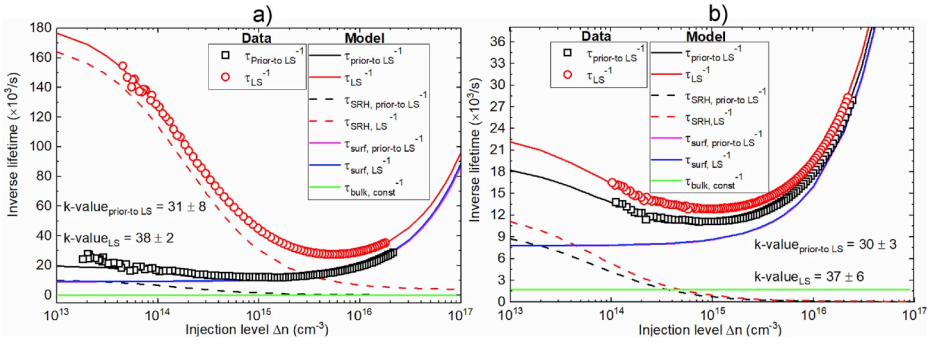

Fig. 7. Injection-dependent lifetime spectroscopy of a) control sample prior to light soaking ($\tau^{-1}_{prior\text{-}to\ LS}$) and after maximum degradation point ($\tau^{-1}_{LS\text{-}19\ h}$). b) sample that underwent a second treatment at 700 °C prior to light soaking ($\tau^{-1}_{prior\text{-}to\ LS}$) and after maximum degradation point ($\tau^{-1}_{LS\text{-}19\ h}$). The fits of the measured data prior to light soaking and at the point of maximum degradation are denoted by the black and red solid lines, respectively. Dashed black and red lines represent fitting metrics of a single level SRH defect component prior to light soaking and at the point of maximum degradation, respectively. Pink, blue and green solid lines denote the fitted surface and bulk components, respectively. These samples were sourced from Manufacturer B. (For interpretation of the references to colour in this figure legend, the reader is referred to the Web version of this article.)

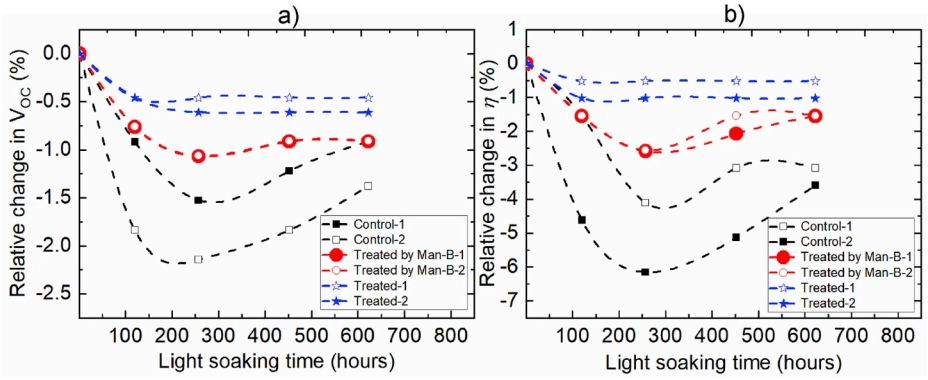

Fig. 8. Change in a) V_{OC} and b) η relative to initial values (as fired, before processing) after light soaking of the full-large area cells. **Control** means the cells did not receive any treatment by neither Manufacturer B nor our method, **Treated by Man-B** means the cells which were treated by Manufacturer B (current injection at elevated temperature), and **Treated** means the cells which were treated by our proposed method in this work. The stability testing condition was 75 °C with an illumination intensity of 1000 W/m^2.

4.2. Stability/instability of the cell after the second annealing step

The second annealing at lower temperatures did not cause any change in the stability of the samples after the defect was de-activated during the first annealing process. This result is consistent with both leading hypotheses for the root cause of LeTID. If the degradation is caused by metal impurities in the bulk (as proposed in Refs. [19,55,56], then the mitigation path will continue to be driven in the same direction during thermal processing at the same temperature. Similarly, if excess hydrogen is the cause, and annealing removes this from the bulk, then further annealing at the same temperature would not be expected to reverse this. In this work, higher temperature annealing was able to reverse the stability and resulted in a re-introduction of LeTID in the bulk. More interestingly, this subsequent degradation was found to be highly non-uniform spatially across the sample and was concentrated in the more dislocated regions of the samples. These regions may have a higher concentration of dissolved impurities [57] and also provide a large number of sites for hydrogen to accumulate [53,58–60]. Future studies into the cause of this bulk degradation for a second annealing step at high temperatures may lead to a deeper understanding of the nature of the LeTID defect.

5. Conclusion

In this work, we propose a two-step process to eliminate LeTID in *p*-type mc-Si PERC solar cells. The first annealing process was shown to improve V_{OC} by ~0.5%$_{rel}$ (~3–4 mV). However, this slow annealing process caused the series resistance and contact resistance to increase by up to a factor of five and three orders of magnitude, respectively. This resulted in a dramatic loss in both efficiency and FF, by up to ~25%$_{rel}$. No significant changes in short-circuit current or pseudo-FF after the first and the second treatments were observed. The second annealing step at a lower temperature (<500 °C) led to a recovery of the loss of cell performance (FF and η), whilst also maintaining the improvement of V_{OC} and the stability of the small area tokens for more than 1700 h of light soaking. A recovery of FF and η was also observed for all the tokens that underwent a second annealing step at higher temperatures >500 °C; however, these conditions caused a reduction in V_{OC}, particularly at the temperature of 700 °C. The reason for the recovery of the FF and η has remained less clear, and future work may be required to do a detailed study of these issues. The changes in V_{OC} after each processing is attributed to the evolution of the bulk lifetime influencing by the post-fire treatment. Additionally, it was shown that if the second annealing was performed at higher temperatures, it would re-activate LeTID, primarily on the dislocations cluster sites. This is possibly due to the high density of impurities which trapped more hydrogen in those regions. These results show that the second annealing process can successfully stabilise the cells; however, careful attention must be paid to annealing parameters. When applying this process on the full-area PERC cells, this process is effective in suppressing the degradation of V_{OC} by ~70%$_{rel}$ and η by up to ~80%$_{rel}$. The proposed approach uses tools directly related to the industrial fabrication of PERC solar cells. This new approach could present a possible pathway to significantly reduce LeTID in industrial *p*-type multi PERC cells.

Declaration of competing interest

The authors declare that they have no known competing financial interests or personal relationships that could have appeared to influence the work reported in this paper.

CRediT authorship contribution statement

Chandany Sen: Conceptualization, Methodology, Software, Validation, Investigation, Data curation, Writing - original draft, Visualization, Writing - review & editing. **Catherine Chan:** Resources, Writing - review & editing, Funding acquisition, Conceptualization. **Phillip Hamer:** Formal analysis, Writing - review & editing, Validation. **Matthew Wright:** Writing - review & editing, Methodology. **CheeMun Chong:** Project administration, Funding acquisition, Resources. **Brett Hallam:** Validation, Writing - review & editing, Resources, Formal analysis, Conceptualization. **Malcolm Abbott:** Resources, Formal analysis, Validation, Project administration, Supervision, Conceptualization.

Acknowledgements

This work was supported by the Australian Government through the Australian Renewable Energy Agency (ARENA 1–A060), the Australian Centre for Advanced Photovoltaics (ACAP, 1-SRI001) and the Australian Research Council through a Discovery Early Career Researcher Award (DE170100620). The responsibility for the views, information, or advice expressed herein is not accepted by the Australian Government. The authors would like to thank Utkarshaa Varshney, Brendan Wright, Daniel Chen, Anastasia Soeriyadi, Bruno Vicari Stefani, Alison Ciesla nee Wenham, Zhuangyi Zhou, Muhammad Umair Khan, Nino Borojevic, Ly Mai, and the support of the Solar Industrial Research Facility for their contributions to useful discussions, data analysis and sample preparation.

Appendix A. Supplementary data

Supplementary data to this article can be found online at https://doi.org/10.1016/j.solmat.2020.110470.

References

[1] K. Ramspeck, S. Zimmermann, H. Nagel, A. Metz, Y. Gassenbauer, B. Birkmann, A. Seidl, S.S. Ag, S. Solar, W. Gmbh, Light induced degradation of rear passivated mc-Si solar cells, in: Proc. 27th Eur. Photovolt. Sol. Conf. Exhib. Frankfurt, Ger., 2012, pp. 861–865.

[2] F. Kersten, P. Engelhart, H.C. Ploigt, A. Stekolnikov, T. Lindner, F. Stenzel, M. Bartzsch, A. Szpeth, K. Petter, J. Heitmann, J.W. Müller, Degradation of multicrystalline silicon solar cells and modules after illumination at elevated temperature, Sol. Energy Mater. Sol. Cells 142 (2015) 83–86.

[3] D. Chen, M. Kim, B.V. Stefani, B.J. Hallam, M.D. Abbott, C.E. Chan, R. Chen, D.N. R. Payne, N. Nampalli, A. Ciesla, T.H. Fung, K. Kim, S.R. Wenham, Evidence of an identical firing-activated carrier-induced defect in monocrystalline and multicrystalline silicon, Sol. Energy Mater. Sol. Cells 172 (2017) 293–300.

[4] J.M. Fritz, A. Zuschlag, D. Skorka, A. Schmid, G. Hahn, Temperature dependent degradation and regeneration of differently doped mc-Si materials, Energy Procedia 124 (2017) 718–725.

[5] H.C. Sio, H. Wang, Q. Wang, C. Sun, W. Chen, H. Jin, D. Macdonald, Light and elevated temperature induced degradation in p-type and n-type cast-grown multicrystalline and mono-like silicon, Sol. Energy Mater. Sol. Cells 182 (2018) 98–104.

[6] F. Fertig, R. Lantzsch, A. Mohr, M. Schaper, M. Bartzsch, D. Wissen, F. Kersten, A. Mette, S. Peters, A. Eidner, J. Cieslak, K. Duncker, M. Junghänel, E. Jarzembowski, M. Kauert, B. Faulwetter-Quandt, D. Meißner, B. Reiche, S. Geißler, S. Hörnlein, C. Klenke, L. Niebergall, A. Schönmann, A. Weihrauch, F. Stenzel, A. Hofmann, T. Rudolph, A. Schwabedissen, M. Gundermann, M. Fischer, J.W. Müller, D.J.W. Jeong, Mass production of p-type Cz silicon solar cells approaching average stable conversion efficiencies of 22 %, Energy Procedia 124 (2017) 338–345.

[7] K. Petter, K. Hübener, F. Kersten, F. Fertig, B. Klöter, J. Müller, H.Q.C. Gmbh, Dependence of LeTID on brick height for different wafer suppliers with several resistivities and dopants, in: 9th Int. Work. Cryst. Silicon Sol. Cell. 6, 2016, p. 6766.

[8] P.V. Magazine, Let's mitigate LID and LeTID, PV mag [Online]. Available at: https://www.pv-magazine-in, 2018.

[9] R. Sharma, A.P. Chong, J.B. Li, A.G. Aberle, Y. Huang, Role of post-metallization anneal sequence and forming gas anneal to mitigate light and elevated temperature induced degradation of multicrystalline silicon solar cells, Sol. Energy Mater. Sol. Cells 195 (2019) 160–167.

[10] REC Group, Combatting LeTID in Multi and Monocrystalline Solar Panels : How Testing Has Demonstrated the High Resistance of REC Solar Panels to LeTID Degradation , Ensuring Long Term Power for Lasting Performance, 2019 ([Online]).

[11] A. Zuschlag, D. Skorka, G. Hahn, Degradation and regeneration in mc-Si after different gettering steps, Prog. Photovoltaics Res. Appl. 25 (2017) 545–552.

[12] J. Lindroos, A. Zuschlag, J. Carstensen, G. Hahn, Light-induced degradation variation in industrial multicrystalline PERC silicon solar cells, in: AIP Conf. Proc. 1999, 2018.

[13] W. Kwapil, T. Niewelt, M.C. Schubert, Kinetics of carrier-induced degradation at elevated temperature in multicrystalline silicon solar cells, Sol. Energy Mater. Sol. Cells 173 (2017) 80–84.

[14] D. Bredemeier, D.C. Walter, R. Heller, J. Schmidt, Impact of hydrogen-rich silicon nitride material properties on light-induced lifetime degradation in multicrystalline silicon, Phys. Status Solidi Rapid Res. Lett. (2019).

[15] A. Herguth, C. Derricks, P. Keller, B. Terheiden, Recovery of LeTID by low intensity illumination: reaction kinetics, completeness and threshold temperature, Energy Procedia 124 (2017) 740–744.

[16] A.E. Morishige, M.A. Jensen, D.B. Needleman, K. Nakayashiki, J. Hofstetter, T.T. A. Li, T. Buonassisi, Lifetime spectroscopy investigation of light-induced degradation in p-type multicrystalline silicon PERC, IEEE J. Photovoltaics. 6 (2016) 1466–1472.

[17] T. Niewelt, F. Schindler, W. Kwapil, R. Eberle, J. Schön, M.C. Schubert, Understanding the light-induced degradation at elevated temperatures: similarities between multicrystalline and floatzone p-type silicon, Prog. Photovoltaics Res. Appl. 26 (2018) 533–542.

[18] D. Bredemeier, D.C. Walter, J. Schmidt, Lifetime degradation in multicrystalline silicon under illumination at elevated temperature: indications for the involvement of hydrogen, in: AIP Conf. Proc. 1999, 2018.

[19] M.A. Jensen, A.E. Morishige, J. Hofstetter, D.B. Needleman, T. Buonassisi, Evolution of LeTID defects in p-type multicrystalline silicon during degradation and regeneration, IEEE J. Photovoltaics 7 (2017) 980–987.

[20] A. Ciesla, S. Wenham, R. Chen, C. Chan, D. Chen, B. Hallam, D. Payne, T. Fung, M. Kim, S. Liu, S. Wang, K. Kim, A. Samadi, C. Sen, C. Vargas, U. Varshney, B. V. Stefani, P. Hamer, N. Nampalli, Z. Hameiri, C. Chong, M. Abbott, Hydrogen-induced degradation, IEEE PVSC (2018).

[21] R. Eberle, W. Kwapil, F. Schindler, M.C. Schubert, S.W. Glunz, Impact of the firing temperature profile on light induced degradation of multicrystalline silicon, Phys. Status Solidi Rapid Res. Lett. 865 (2016) 861–865.

[22] M.A. Jensen, A. Zuschlag, S. Wieghold, D. Skorka, A.E. Morishige, G. Hahn, T. Buonassisi, Evaluating root cause: the distinct roles of hydrogen and firing in activating light- and elevated temperature-induced degradation, J. Appl. Phys. 124 (2018).

[23] T.H. Fung, M. Kim, D. Chen, C.E. Chan, B.J. Hallam, R. Chen, D.N.R. Payne, A. Ciesla, S.R. Wenham, M.D. Abbott, A four-state kinetic model for the carrier-induced degradation in multicrystalline silicon : introducing the reservoir state, Sol. Energy Mater. Sol. Cells 184 (2018) 48–56.

[24] U. Varshney, M. Abbott, A. Ciesla, D. Chen, S. Liu, C. Sen, M. Kim, S. Wenham, B. Hoex, C. Chan, Evaluating the impact of SiNx thickness on lifetime degradation in silicon, IEEE J. Photovoltaics 9 (2019) 601–607.

[25] D.N.R. Payne, C.E. Chan, B.J. Hallam, B. Hoex, M.D. Abbott, S.R. Wenham, D. M. Bagnall, Rapid passivation of carrier-induced defects in p-type multi-crystalline silicon, Sol. Energy Mater. Sol. Cells 158 (2016) 102–106.

[26] K. Kraus, A.A. Brand, F. Fertig, S. Rein, J. Nekarda, Fast regeneration processes to avoid light-induced degradation in multicrystalline silicon solar cells, 2017 IEEE 44th Photovolt, in: Spec. Conf. PVSC 6, 2017, pp. 1–3, 2018.

[27] C.E. Chan, D.N.R. Payne, B.J. Hallam, M.D. Abbott, T.H. Fung, A.M. Wenham, B. S. Tjahjono, S.R. Wenham, Rapid stabilization of high-performance multicrystalline P-type silicon PERC cells, IEEE J. Photovoltaics. 6 (2016) 1473–1479.

[28] K. Nakayashiki, J. Hofstetter, A.E. Morishige, T.T.A. Li, D.B. Needleman, M. A. Jensen, T. Buonassisi, Engineering solutions and root-cause analysis for light-induced degradation in p-type multicrystalline silicon PERC modules, IEEE J. Photovoltaics. 6 (2016) 860–868.

[29] D. Bredemeier, D. Walter, S. Herlufsen, J. Schmidt, Lifetime degradation and regeneration in multicrystalline silicon under illumination at elevated temperature, AIP Adv. 6 (2016).

[30] P. Engelhart, F. Kersten, Method of producing solar cells, Patent 27 (2013). DE102013113108.5A.

[31] P. Engelhart, F. Kersten, Solar cell manufacturing process and solar cell treatment process, Patent 27 (2013). DE102013113123.9A.

[32] C. Vargas, K. Kim, G. Coletti, D. Payne, C. Chan, S. Wenham, Z. Hameiri, Carrier-induced degradation in multicrystalline silicon: dependence on the silicon nitride passivation layer and hydrogen released during firing, IEEE J. Photovoltaics. 8 (2018) 413–420.

[33] D. Bredemeier, D.C. Walter, J. Schmidt, Possible candidates for impurities in mc-Si wafers responsible for light-induced lifetime degradation and regeneration, Sol. RRL. 2 (2018) 1700159.

[34] C. Sen, C. Chan, P. Hamer, M. Wright, U. Varshney, S. Liu, D. Chen, A. Samadi, A. Ciesla, C.M. Chong, B. Hallam, M. Abbott, Annealing prior to contact firing: a potential new approach to suppress LeTID, Sol. Energy Mater. Sol. Cells 200 (2019) 109938.

[35] C. Sen, M. Kim, D. Chen, U. Varshney, S. Liu, A. Samadi, A. Ciesla, S.R. Wenham, C. E. Chan, C. Chong, M.D. Abbott, B.J. Hallam, Assessing the impact of thermal profiles on the elimination of light- and elevated-temperature-induced degradation, IEEE J. PHOTOVOLTAICS 9 (2019) 40–48.

[36] M. Yli-Koski, T.P. Pasanen, I. Heikkinen, M. Serué, H. Savin, Low-T anneal as cure for LeTID in Mc-Si PERC cells, in: 15th Int. Conf. Conc. Photovolt. Syst. 2149, 2019, p. 140013.

[37] R. Sharma, A.G. Aberle, J.B. Li, Optimization of Belt Furnace Anneal to Reduce Light and Elevated Temperature Induced Degradation of Effective Carrier Lifetime of P-type Multicrystalline Silicon Wafers, 2018, pp. 1–8, 1800070.

[38] C. Chan, P. Hamer, G. Bourret-Sicotte, R. Chen, A. Ciesla, B. Hallam, D. Payne, R. S. Bonilla, S. Wenham, Instability of increased contact resistance in silicon solar cells following post-firing thermal processes, Sol. RRL. 1700129 (2017) 1700129.

[39] P. Hamer, C. Chan, R.S. Bonilla, B. Hallam, G. Bourret-Sicotte, K.A. Collett, S. Wenham, P.R. Wilshaw, Hydrogen induced contact resistance in PERC solar cells, Sol. Energy Mater. Sol. Cells 184 (2018) 91–97.

[40] A. Peral, A. Dastgheib-Shirazi, V. Fano, J.C. Jimeno, G. Hahn, C. Del Cañizo, Impact of extended contact cofiring on multicrystalline silicon solar cell parameters, IEEE J. Photovoltaics. 7 (2017) 91–96.

[41] P. Hamer, H. Li, C. Chan, C. Sen, R.S. Bonilla, P. Wilshaw, The behavior and transport of hydrogen in silicon solar cells observed through changes in contact resistance, 7th world, in: Conf. Photovolt. Energy Convers., 2018, pp. 5–7.

[42] R. Sinton, A. Cuevas, A quasi-steady-state open-circuit voltage method for solar cell characterization, in: 16th Eur. Photovolt. Sol. Energy Conf., 2000, pp. 1–4.

[43] D. Pysch, A. Mette, S.W. Glunz, A review and comparison of different methods to determine the series resistance of solar cells, Sol. Energy Mater. Sol. Cells 91 (2007) 1698–1706.

[44] D.L. Meier, D.K. Schroder, Contact resistance: its measurement and relative importance to power loss in a solar cell, IEEE Trans. Electron. Dev. 31 (1984) 647–653.

[45] R.A. Sinton, A. Cuevas, Contactless determination of current-voltage characteristics and minority-carrier lifetimes in semiconductors from quasi-steady-state photoconductance data, Appl. Phys. Lett. 69 (1996) 2510–2512.

[46] H. Nagel, C. Berge, A.G. Aberle, Generalized analysis of quasi-steady-state and quasi-transient measurements of carrier lifetimes in semiconductors, J. Appl. Phys. 86 (1999) 6218–6221.

[47] A. Richter, F. Werner, A. Cuevas, J. Schmidt, S.W. Glunz, Improved parameterization of Auger recombination in silicon, Energy Procedia 27 (2012) 88–94.

[48] D.N.R. Payne, C. Vargas, Z. Hameiri, S.R. Wenham, D.M. Bagnall, An advanced software suite for the processing and analysis of silicon luminescence images, Comput. Phys. Commun. 215 (2017) 223–234.

[49] A. Herguth, G. Hahn, Temperature induced degradation of the contact resistance of Ag-screen printed p-type silicon solar cells, in: EU-PVSEC 24th, 2009, pp. 2012–2014.

[50] J. Asensio-Lozano, G. Vander Voort, The Al-Si phase diagram, TECH NOTES. 5 (n. d.) 5–9.

[51] S. Liu, D. Payne, C. Vargas Castrillon, D. Chen, M. Kim, C. Sen, U. Varshney, Z. Hameiri, C. Chan, M. Abbott, S. Wenham, Impact of dark annealing on the kinetics of light- and elevated-temperature-induced degradation, IEEE J. Photovoltaics (2018) 1–9.

[52] P. Hamer, B. Hallam, S. Wenham, M. Abbott, Manipulation of hydrogen charge states for passivation of P-type wafers in photovoltaics, IEEE J. Photovoltaics 4 (2014) 1252–1260.

[53] A. Samadi, C. Sen, S. Liu, U. Varshney, D. Chen, M. Kim, A. Soufiani, M. Contreras, C. Chong, A. Ciesla, M. Abbott, C. Chan, Hydrogenation of Dislocations in P-type Cast-Mono Silicon vol 140007, 2019, p. 2052.

[54] M.A. Jensen, A.E. Morishige, J. Hofstetter, D.B. Needleman, T. Buonassisi, Evolution of p-type LeTID defects in multicrystalline silicon during degradation and regeneration, IEEE J. Photovoltaics 7 (2016) 1–8.
[55] J. Schmidt, D. Bredemeier, D.C. Walter, On the defect physics behind light and elevated temperature-induced degradation (LeTID) of multicrystalline silicon solar cells, IEEE J. Photovoltaics (2019) 1–7.
[56] A. Schmid, A. Zuschlag, D. Skorka, J. Fritz, C. Winter, G. Hahn, Influence of different transition metal contaminations on degradation, in: 33rd Eur. Photovolt. Sol. Energy Conf., 2017, pp. 321–324.
[57] S.A. McHugo, A.C. Thompson, A. Mohammed, G. Lamble, I. Périchaud, S. Martinuzzi, M. Werner, M. Rinio, W. Koch, H.U. Hoefs, C. Haessler, Nanometer-scale metal precipitates in multicrystalline silicon solar cells, J. Appl. Phys. 89 (2001) 4282–4288.
[58] D. Tweddle, P. Hamer, Z. Shen, V.P. Markevich, M.P. Moody, P.R. Wilshaw, Direct observation of hydrogen at defects in multicrystalline silicon, Prog. Photovoltaics Res. Appl. (2019) 1–7.
[59] C.E. Dubé, J.I. Hanoka, Hydrogen passivation of multicrystalline silicon, in: Conf. Rec. IEEE Photovolt. Spec. Conf., 2005, pp. 883–888.
[60] A. Wenham, L. Song, M. Abbott, I. Zafirovska, S. Wang, B. Hallam, C. Chan, A. Barnett, S. Wenham, Defect passivation on cast-mono crystalline screen-printed cells, Front. Energy 11 (2017) 60–66.
[61] C. Sen, C. Chan, D. Chen, M. Wright, U. Varshney, M. Kim, A. Samadi, S. Liu, A. Ciesla, C. Chong, B. Hallam, M. Abbott, Different Extent and Behaviour of LeTID in the Past and Current PERC Silicon Solar Cells, Asia-Pacific Solar Research Conference (2019).